

Electron-beam-induced current measurements with applied bias provide insight to locally resolved acceptor concentrations at p - n junctions

Cite as: AIP Advances 5, 077191 (2015); <https://doi.org/10.1063/1.4928097>

Submitted: 22 June 2015 . Accepted: 23 July 2015 . Published Online: 31 July 2015

D. Abou-Ras, N. Schäfer, N. Baldaz, S. Brunken, and C. Boit



View Online



Export Citation



CrossMark

ARTICLES YOU MAY BE INTERESTED IN

[Charge collection scanning electron microscopy](#)

Journal of Applied Physics **53**, R51 (1982); <https://doi.org/10.1063/1.331667>

[Depletion region surface effects in electron beam induced current measurements](#)

Journal of Applied Physics **120**, 095702 (2016); <https://doi.org/10.1063/1.4962016>

[Evaluation of diffusion lengths and surface recombination velocities from electron beam induced current scans](#)

Applied Physics Letters **43**, 120 (1983); <https://doi.org/10.1063/1.94139>

AVS Quantum Science

Co-Published by



RECEIVE THE LATEST UPDATES



Electron-beam-induced current measurements with applied bias provide insight to locally resolved acceptor concentrations at *p-n* junctions

D. Abou-Ras,^{1,a} N. Schäfer,¹ N. Baldaz,¹ S. Brunken,¹ and C. Boit²

¹Helmholtz-Zentrum Berlin für Materialien und Energie, Hahn-Meitner-Platz 1, 14109 Berlin, Germany

²Technische Universität Berlin, Department of Semiconductor Devices, Einsteinufer 19, 10587 Berlin, Germany

(Received 22 June 2015; accepted 23 July 2015; published online 31 July 2015)

Electron-beam-induced current (EBIC) measurements have been employed for the investigation of the local electrical properties existing at various types of electrical junctions during the past decades. In the standard configuration, the device under investigation is analyzed under short-circuit conditions. Further insight into the function of the electrical junction can be obtained when applying a bias voltage. The present work gives insight into how EBIC measurements at applied bias can be conducted at the submicrometer level, at the example of CuInSe₂ solar cells. From the EBIC profiles acquired across ZnO/CdS/CuInSe₂/Mo stacks exhibiting *p-n* junctions with different net doping densities in the CuInSe₂ layers, values for the width of the space-charge region, *w*, were extracted. For all net doping densities, these values decreased with increasing applied voltage. Assuming a linear relationship between *w*² and the applied voltage, the resulting net doping densities agreed well with the ones obtained by means of capacitance-voltage measurements. © 2015 Author(s). All article content, except where otherwise noted, is licensed under a Creative Commons Attribution 3.0 Unported License. [<http://dx.doi.org/10.1063/1.4928097>]

Electron-beam-induced current (EBIC) in a scanning electron microscope is established as a standard tool for analysis of local short-circuit current densities at electrical junctions.^{1,2} When collecting the EBIC signals from a semiconductor device such as a single *p-n* junction solar cell, the analysis may be performed with the electron beam impinging on the front contact,^{3,4} on the back contact,^{5,6} or on the cross-section of the device.⁷ Evaluation of EBIC data acquired on single *p-n* junction solar cells using these measurement geometries can deliver values for the width *w* of the space-charge region (SCR), the minority carrier diffusion length in the quasi-neutral part of the solar absorber, as well as the recombination velocities at the contacts and at the investigated surface of the specimen.^{7–10}

Most EBIC measurements at solar cells have been conducted under short-circuit condition, which does not correspond to the device operation under sun light. Therefore, further insight into the electrical properties of the device may be obtained when applying a bias voltage.¹¹ However, this approach may bring about background currents, superimposing the EBIC and being larger by several orders of magnitude (μA to mA vs. nA). There is a need for the lock-in amplification of the EBIC signal.¹² When evaluating the EBIC profiles across junctions of solar cells with *p-n*⁺ characteristics (where the doping level of the *n*-type part of the junction is substantially higher than that of the *p*-type part) at various bias voltages, the width *w* of the SCR should decrease with increasing bias voltage *V*_a according to¹³

$$w = (2\epsilon_r\epsilon_0(V_b - V_a)/eN_A)^{0.5}, \quad (1)$$

^aCorresponding author: daniel.abou-ras@helmholtz-berlin.de

where ϵ , ϵ_0 , V_b , e , and N_A are the dielectric susceptibilities of the investigated material and the vacuum, the build-in potential of the junction, the elemental charge, and the net doping of the p -type part of the junction. Note that this equation is valid only assuming that the SCR is fully depleted, that the quasi-neutral region is indeed charge-neutral, and that N_A is constant throughout the p -type part. These assumptions are generally not valid for real solar-cell devices.

The present work provides EBIC measurements with applied bias on CuInSe₂ thin-film solar cells. These devices consist of thin-film stacks with total thicknesses of only a few micrometers. Therefore, they pose a considerable challenge in terms of spatial resolution of the EBIC signals. Reports on EBIC measurements under short-circuit conditions performed on CuInSe₂ solar cells were published by several groups.¹⁴⁻¹⁷ Only a few publications¹⁸ dealt with EBIC at applied bias voltages, while EBIC signals across the p - n junction were evaluated only qualitatively, without extracting electrical parameters. The present work aims at modeling the acquired EBIC profiles across the p - n junction on cross-sectional samples, with the focus of obtaining values for the width of the SCR, w . The first objective is to give a proof of concept in terms of verifying the trend of decreasing w with increasing bias voltage V_a , the second to extract values for the build-in potential V_b and the net doping N_A using Eq. (1), and to compare the N_A values with corresponding measurements by means of capacitance-voltage profiling.

CuInSe₂ thin films were deposited on Mo-coated glass substrates by a three-stage coevaporation process.¹⁹ The doping level in CuInSe₂ can be controlled by introducing different amounts of NaF into the layer, either as precursor prior to the deposition, or by a post-deposition treatment. In the present work, three different CuInSe₂ thin films were fabricated:

- a Na-free CuInSe₂ layer, leading to a nominal net-doping level in CuInSe₂ of 10^{14} cm⁻³.
- one with an additional, 12 nm thick NaF layer deposited on the CuInSe₂/Mo/glass stack, annealed at an elevated temperature, leading to a nominal net-doping level in CuInSe₂ of 10^{15} cm⁻³.
- one with a 12 nm thick NaF precursor layer prior to the deposition of CuInSe₂, leading to a nominal net-doping level in CuInSe₂ of 10^{16} cm⁻³.

Further details can be found in Ref. 20. Solar cells were completed by a CdS buffer layers via chemical bath deposition and by a i-ZnO/ZnO:Al bilayer via sputter-deposition. The photovoltaic performances of the three solar-cell with the different doping levels in the CuInSe₂ layers are given in Table I.

Capacitance-voltage measurements were performed at room temperature using an HP4284 LCR-Meter and frequencies of 100 kHz. The capacitance values were calculated assuming a simply RC circuit.

EBIC analyses were conducted using a Zeiss UltraPlus scanning electron microscope, equipped with a beam blanker and an EBIC amplifier by point electronic GmbH. For these analyses, cross-sectional specimens of the CuInSe₂ solar cells given in Table I were fractured. For each doping level, 3 specimens were measured. The EBIC signals were recorded by means of the acquisition and evaluation software DIPS (point electronic GmbH), which also controls the applied bias voltage. In order to avoid high-injection conditions,²¹ beam currents of only few pA for the impinging electron beam were used. The beam energies were kept small at 3-7 kV, for best spatial resolutions. The frequency of the beam blanker was chosen between 10 and 40 kHz, for sample areas of 4-9 mm². The time constant of the lock-in amplifier was 3 ms, i.e., about three times smaller than the frequency of the beam blanker. For each pixel, a dwell-time of 1.1 ms was selected. As a result, the amplified

TABLE I. Overview of studied CuInSe₂ solar cells and their photovoltaic parameters (best cells; V_{oc} : open-circuit voltage, j_{sc} : short-circuit current density, FF : fill factor, η : power-conversion efficiency).

Nominal doping level (cm ⁻³)	V_{oc} (mV)	j_{sc} (mA/cm ²)	FF (%)	η (%)
10^{14}	317	38.9	64	7.8
10^{15}	451	40.8	74	13.6
10^{16}	459	38.1	71	12.4

EBIC signal was integrated across about 3 pixels. The gain was about 7×10^4 . The SEM and the EBIC images were recorded on areas of 250×25 pixels.

It was found that for values outside a certain range of bias voltages, the EBIC profiles exhibited shapes with very large SCR widths and increased diffusion lengths, which were not able to be described by the model outlined below and persisted also after changing the bias voltage back to a different value. For the 10^{15} and 10^{16} cm^{-3} samples, this range was about -0.1 to 0.4 V , for the 10^{14} cm^{-3} sample about -0.05 to 0.15 V . This behavior can be attributed to a persistent irradiation effect, as outlined by Kniese *et al.*,¹⁶ which is more pronounced for the solar cell with a considerably low doping level (10^{14} cm^{-3}) in the CuInSe₂ layer.

The EBIC simulations were conducted based on the one-dimensional, analytical model proposed by Donolato.⁷ It is assumed that the EBIC signals do not vary substantially parallel to the p - n junction but only perpendicular to it. The EBIC value $I(a)$ measured when the electron beam impinges on the solar-cell cross-section at position a can be regarded as the convolution of generation profile $g(x, a)$ and the collection function $f_c(x)$, where x is the position of generation of electron-hole pairs upon electron irradiation:

$$I(a) = \int_{-\infty}^{\infty} g(x, a) f_c(x) dx. \quad (2)$$

Note that $g(x, a)$ and $f_c(x)$ are generally not independent.²² Still, for the sake of simplicity, we assume independency in order to be able to apply Eq. (2) for the simulation of the EBIC profiles. The generation profile $g(x, a)$ can be approximated by an empirical expression.¹⁵ The collection function $f_c(x)$ was divided into three parts (where $x = 0$ is set to the CdS/CuInSe₂ interface):

- for all x within the SCR (of width w), $f_c(x)$ is assumed to be 1

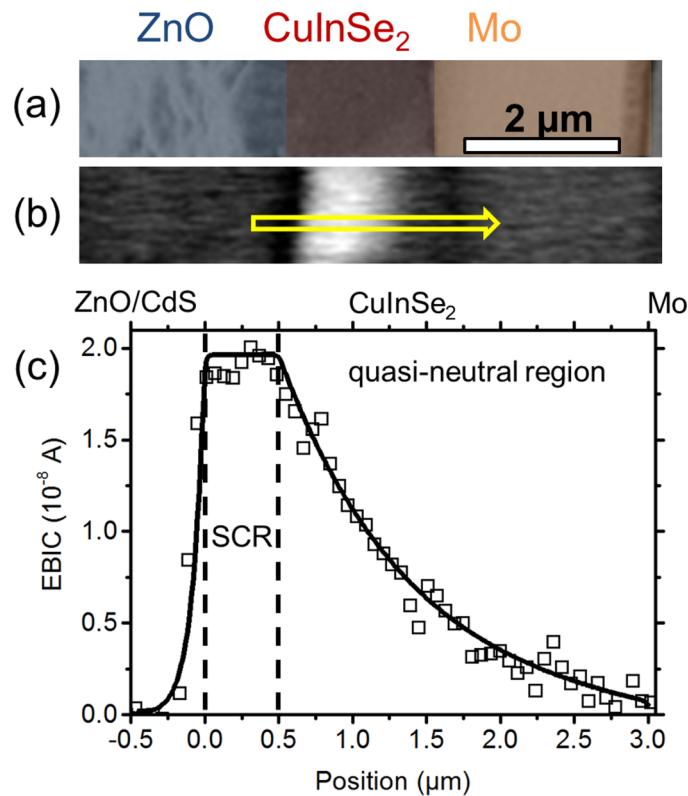


FIG. 1. Exemplary EBIC measurement and the simulation of the acquired EBIC profile. (a) SEM image of a ZnO/CdS/CuInSe₂/Mo/glass cross-section with a nominal net doping density in the CuInSe₂ layer of 10^{14} cm^{-3} . (b) Corresponding EBIC image acquired at zero bias. (c) Measured EBIC profile (open squares) extracted along the yellow arrow in (b) and the simulated EBIC signal (solid line).

- for the CdS/ZnO buffer/window region, $f_c(x) = \exp(-|x|/L_p)$ (L_p is the diffusion length of holes in the CdS/ZnO region)
- for the quasi-neutral region in the CuInSe₂ absorber layer,

$$f_c(x) = \frac{\frac{1}{L_n} \cosh\left(\frac{x-x_{M0}}{L_n}\right) - \frac{S_{M0}}{D_n} \sinh\left(\frac{x-x_{M0}}{L_n}\right)}{\frac{S_{M0}}{D_n} \sinh\left(\frac{x_{M0}-x_{SCR}}{L_n}\right) + \frac{1}{L_n} \cosh\left(\frac{x_{M0}-x_{SCR}}{L_n}\right)},$$

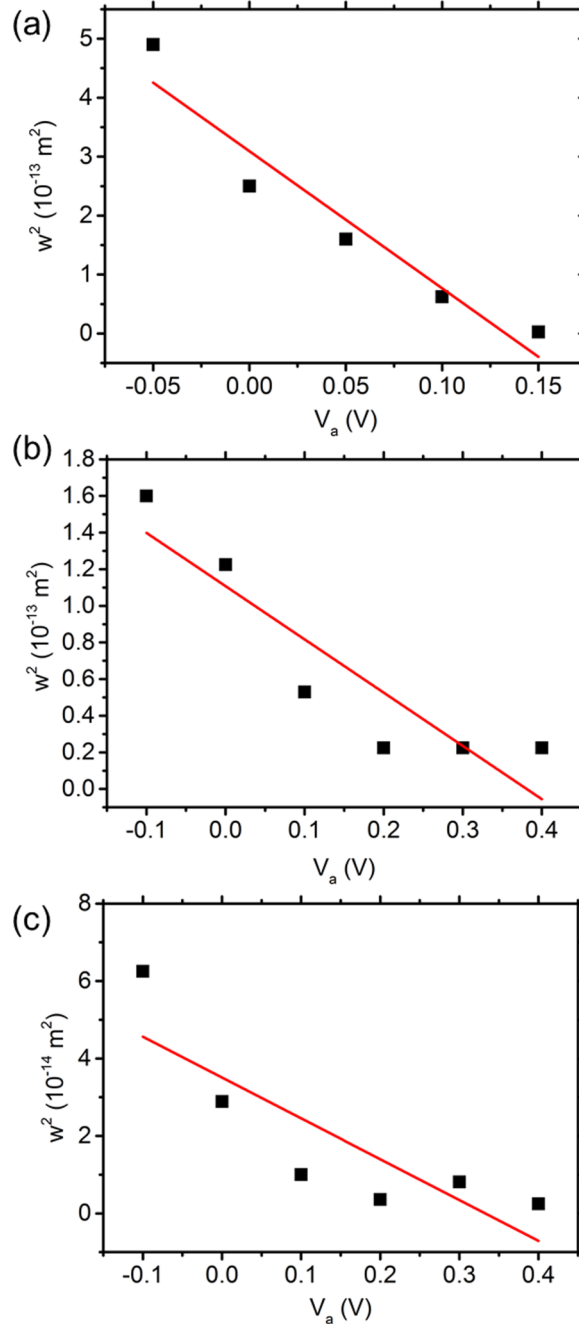


FIG. 2. The square of the width of the SCR, w^2 , as a function of the applied bias, V_a , for the three investigated solar-cell samples with nominal doping densities of (a) 10^{14} , (b) 10^{15} , and (c) 10^{16} cm^{-3} in the CuInSe₂ layers. The measured values are given as solid squares, the linear fits are represented by solid red lines.

where L_n and D_n are the diffusion length and diffusion constant of the electrons in the CuInSe₂ absorber layer, S_{Mo} is the recombination velocity at the Mo back contact, and x_{Mo} and x_{SCR} are the positions of the Mo back contact and the edge of the SCR. In order to fit the simulated to the experimental EBIC profiles, w (equivalent to x_{SCR}), x_{Mo} , L_p , L_n , and D_n are used as parameters (where w and L_n exhibit the largest impact).

An exemplary EBIC measurement and the simulation of the acquired EBIC profile are given in Fig. 1, where a SEM image (Fig. 1(a)), an EBIC image (Fig. 1(b)), and an extracted EBIC profile across the ZnO/CdS/CuInSe₂/Mo/glass stack is presented, along with the corresponding simulated EBIC signal (Fig. 1(c)). Note that all EBIC profiles acquired on the three solar-cell samples listed in Table I at various bias voltages are provided in Ref. 23.

The squares of the widths of the SCR, w^2 , were plotted as a function of the applied bias, V_a , for the three investigated solar-cell samples (Fig. 2). Indeed, decreasing widths of the SCR with increasing applied bias for all three solar-cell samples were found, which is according to Eq. (1). Therefore, the first objective of the present work was achieved.

In addition, the dependencies of w^2 vs. V_a were fitted using a linear function and $\epsilon_r = 13.6$ (Ref. 24), in order to determine the build-in potentials. It is clear from Figs. 2(a)–2(c) that the values of w^2 vs. V_a do not exhibit a linear relationship for the complete voltage range. However, a linear relationship is assumed in order to extract values for V_b and N_A , which are given in Table II. This is justified since the R^2 values²⁵ for the three linear fits range from 0.65 to 0.90, i.e., they are closer to 1 than to 0.

The extracted V_b values are slightly smaller than those calculated by²⁶

$$V_b = k_B T / e \ln(N_D N_A / n_i^2) \quad (3)$$

(where k_B is the Boltzmann constant, T the absolute temperature, 300 K, N_D the donor concentration in the window layer, $N_D = 1 \times 10^{18} \text{ cm}^{-3}$ (Ref. 27), and n_i the intrinsic carrier density, $n_i = 5 \times 10^9 \text{ cm}^{-3}$ (Ref. 27)), which are in the range of 0.5–0.6 V. The deviations of the theoretical from the experimental values can be explained by the inaccuracy of the applied model (see discussions to Eq. (1) above) and also by the fact that Eq. (3) is valid only for homojunctions, while for the present case of ZnO/CdS/CuInSe₂ heterojunctions, also electronic band offsets have to be considered.

The results from capacitance-voltage measurements on the same identical solar cells are given in Fig. 3. In the Mott-Schottky plots (Fig. 3(a)), the capacitance C is related to the applied voltage V_a via $C^{-2} = 2(V_b - V_a) / (\epsilon_r \epsilon_0 e N_A)$. This is, N_A and V_b were determined by a linear fit of $C^{-2}(V_a)$ and represented in Table II.

The net doping densities in Fig. 3(b) were calculated by derivation of the Mott-Schottky plots in Fig. 3(a). Since with varying applied bias voltage, the edge of the SCR in the CuInSe₂ absorber layer shifts basically from close to the Mo back contact (for large negative V_a) to close to the CdS buffer layer (for large positive V_a), Fig. 3(b) can be interpreted in terms of a spatial doping distribution perpendicular to the p - n junction. Apparently, the net doping densities N_A are not constant across the CuInSe₂ absorber layer. Nevertheless, the values obtained by EBIC and C-V measurements are in good agreement (Table II).

It should be noted that the determination of the net doping densities N_A from EBIC measurements by use of Eq. (1) can by no means replace capacitance-voltage analysis as standard technique

TABLE II. Values for the build-in potential V_b and the net doping N_A , determined from EBIC measurements, capacitance-voltage analysis, as well as by use of Eq. (3). We note that the nominal doping level is to be considered as order of magnitude.

Nominal doping level (cm^{-3})	N_A from EBIC (cm^{-3})	N_A from C-V (cm^{-3})	V_b from EBIC (V)	V_b from C-V (V)	V_b from Eq. (3) (V)
10^{14}	$(7 \pm 3) \times 10^{14}$	$(3 \pm 1) \times 10^{14}$	0.2 ± 0.1	0.2 ± 0.1	0.5
10^{15}	$(5 \pm 2) \times 10^{15}$	$(4 \pm 1) \times 10^{15}$	0.4 ± 0.1	0.4 ± 0.1	0.6
10^{16}	$(1 \pm 0.4) \times 10^{16}$	$(3 \pm 1) \times 10^{16}$	0.3 ± 0.1	0.7 ± 0.2	0.7

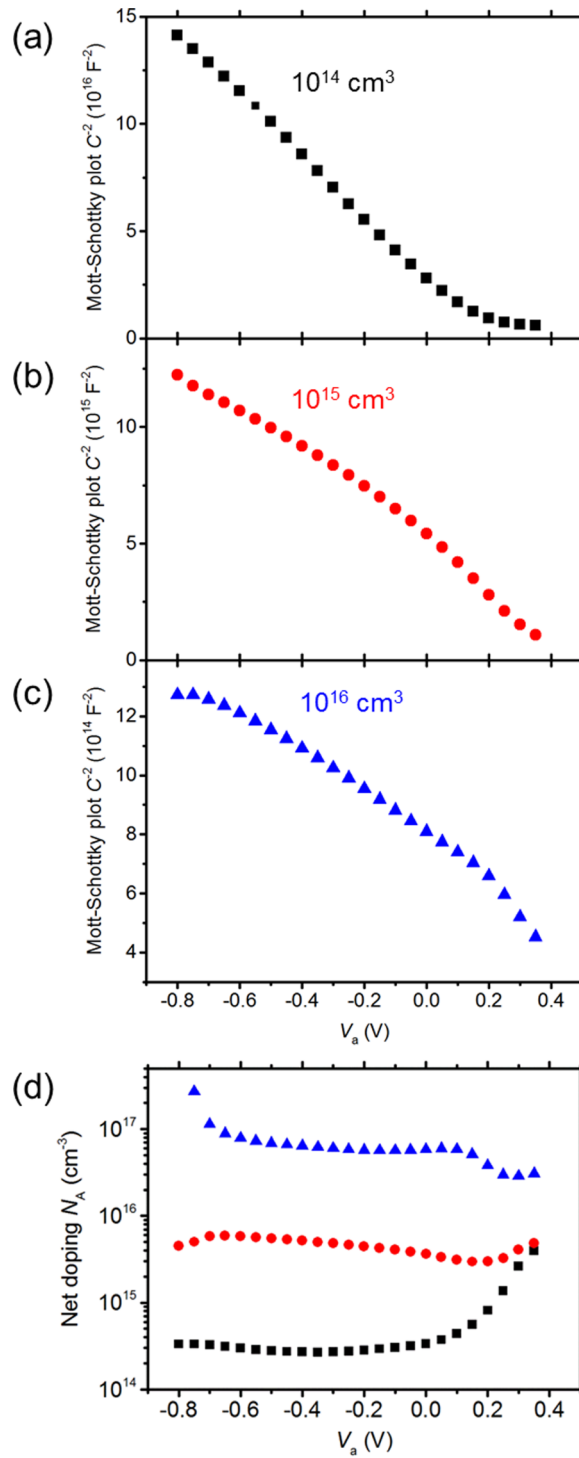


FIG. 3. (a-c) Mott-Schottky plots for the three CuInSe₂ solar-cell samples, in which their nominal doping densities are indicated. (d) Net doping densities N_A as functions of the applied bias voltage V_a , calculated from the Mott-Schottky plots in (a-c).

for this purpose. However, while C-V measurements give insight to spatial doping distributions *perpendicular* to the p - n junction, EBIC profiles extracted along a cross-section of a solar cell provide access to these distributions *parallel* to the p - n junction. Both techniques are thus complementary.

In conclusion, EBIC measurements were performed at applied bias on CuInSe₂ solar cells containing absorber layers with different net doping densities. The acceptor concentrations extracted from EBIC profiles agreed well with values determined by means of capacitance-voltage measurements. The proposed approach can be applied to further semiconductor devices, as long as doping levels and thicknesses of the active layers are still appropriate, with respect to the spatial resolution of EBIC measurements at low electron-beam energies, which can be considered to be in the order of few tens of nanometers.

ACKNOWLEDGEMENTS

The authors are grateful to Carola Ferber, Michael Kirsch, Tim Münchenberg, Jakob Lauche, and Karsten Prietzel, all HZB, for help with the solar-cell production. The collaboration with point electronic GmbH, Halle, Germany, is gratefully acknowledged. Special thanks are due to Thomas Unold, HZB, for fruitful discussions. The present work was supported by the Helmholtz Virtual Institute “Microstructure Control for Thin-Film Solar Cells” (VH-VI-520).

- ¹ H.J. Leamy, *J. Appl. Phys.* **53**, R51 (1982).
- ² *SEM Microcharacterization of Semiconductors*, edited by D.B. Holt and D.C. Joy (Academic Press, London, 1989).
- ³ R. Scheer, C. Knieper, and L. Stolt, *Appl. Phys. Lett.* **67**, 3007 (1995).
- ⁴ O. Breitenstein, J. Bauer, and J. P. Rakotoniaina, *Semiconductors* **41**, 440 (2007).
- ⁵ O. Breitenstein, J. Bauer, M. Kittler, T. Arguirov, and W. Seifert, *Scanning* **30**, 331 (2008).
- ⁶ J. Kavalakkatt, D. Abou-Ras, J. Haarstrich, C. Ronning, M. Nichterwitz, R. Caballero, T. Rissom, T. Unold, R. Scheer, and H. W. Schock, *J. Appl. Phys.* **115**, 014504 (2014).
- ⁷ C. Donolato, *Appl Phys Lett* **43**, 120 (1983).
- ⁸ C. Donolato, *phys. stat. sol. (a)* **65**, 649 (1981).
- ⁹ K.L. Luke, O. von Roos, and L. Cheng, *J. Appl. Phys.* **57**, 1978 (1985).
- ¹⁰ R. Scheer, *Solid State Phen.* **67-68**, 57 (1999).
- ¹¹ N.C. MacDonald and T.E. Everhart, *Appl. Phys. Lett.* **7**, 267 (1965).
- ¹² T. Sekiguchi and K. Sumino, *Rev. Sci. Instrum.* **66**, 4277 (1995).
- ¹³ S.M. Sze, *Physics of semiconductor devices* (Wiley, New York, 1981).
- ¹⁴ R. Scheer, M. Wilhelm, H.J. Lewerenz, H.W. Schock, and L. Stolt, *Sol. En. Mater. Sol. Cells* **49**, 299 (1997).
- ¹⁵ J. Rechid, A. Kampmann, and R. Reineke-Koch, *Thin Solid Films* **361-362**, 198 (2000).
- ¹⁶ R. Kniese, M. Powalla, and U. Rau, *Thin Solid Films* **515**, 6163 (2007).
- ¹⁷ M. Nichterwitz, R. Caballero, C.A. Kaufmann, H.-W. Schock, and T. Unold, *J. Appl. Phys.* **113**, 044515 (2013).
- ¹⁸ A. Harb, Bachelor thesis, KIT, Karlsruhe, Germany, 2014.
- ¹⁹ R. Caballero, C.A. Kaufmann, V. Efimova, T. Rissom, V. Hoffmann, and H. W. Schock, *Progr. Photovolt.: Res. Appl.* **21**, 30 (2013).
- ²⁰ S. Brunken, D. Greiner, H. Allaf Navirian, C.A. Kaufmann, and T. Unold, in *Conference Record of the 40th IEEE Photovoltaic Specialists Conference and Exhibition, Denver, CO, USA, June 8-13, 2014*. p. 3629.
- ²¹ M. Nichterwitz and T. Unold, *J. Appl. Phys.* **114**, 134504 (2013).
- ²² M. Nichterwitz, R. Caballero, C.A. Kaufmann, H.-W. Schock, and T. Unold, *J. Appl. Phys.* **113**, 044515 (2013).
- ²³ See supplementary material at <http://dx.doi.org/10.1063/1.4928097> for all measured and simulated EBIC profiles for various applied voltages and doping levels in the CuInSe₂ layers.
- ²⁴ P.W. Li, R.A. Anderson, and R.H. Plovnick, *J. Phys. Chem. Solids* **40**, 333 (1979).
- ²⁵ M.H. Kutner, C.J. Nachtsheim, J. Neter, and W. Li, *Applied linear statistical models*, 5th ed. (McGrawHill/Irwin, New York, 2005).
- ²⁶ A.L. Fahrenbruch and R.H. Bube, *Fundamentals of solar cells: Photovoltaic solar energy conversion* (Academic Press, New York, 1983).
- ²⁷ R. Scheer and H.-W. Schock, *Chalcogenide Photovoltaics: Physics, Technologies, and Thin Film Devices* (Wiley-VCH, Weinheim, 2011).